ADVANCED MATERIALS
www.advmat.de

Overcoming the Limitations of MXene Electrodes for Solution-Processed Optoelectronic Devices

Huanyu Zhou, Shin Jung Han, Hyeon-Dong Lee, Danzhen Zhang, Mark Anayee, Seung Hyeon Jo, Yury Gogotsi, and Tae-Woo Lee**

MXenes constitute a rapidly growing family of 2D materials that are promising for optoelectronic applications because of numerous attractive properties, including high electrical conductivity. However, the most widely used titanium carbide ($Ti_3C_2T_x$) MXene transparent conductive electrode exhibits insufficient environmental stability and work function (*WF*), which impede practical applications $Ti_3C_2T_x$ electrodes in solution-processed optoelectronics. Herein, $Ti_3C_2T_x$ MXene film with a compact structure and a perfluorosulfonic acid (PFSA) barrier layer is presented as a promising electrode for organic light-emitting diodes (OLEDs). The electrode shows excellent environmental stability, high *WF* of 5.84 eV, and low sheet resistance R_S of 97.4 Ω sq^{-1}. The compact $Ti_3C_2T_x$ structure after thermal annealing resists intercalation of moisture and environmental contaminants. In addition, the PFSA surface modification passivates interflake defects and modulates the *WF*. Thus, changes in the *WF* and R_S are negligible even after 22 days of exposure to ambient air. The $Ti_3C_2T_x$ MXene is applied for large-area, 10 × 10 passive matrix flexible OLEDs on substrates measuring 6 × 6 cm. This work provides a simple but efficient strategy to overcome both the limited environmental stability and low *WF* of MXene electrodes for solution-processable optoelectronics.

1. Introduction

MXenes are 2D transition metal carbides, nitrides, or carbonitrides. MXenes have high electrical conductivity (σ) and superior optical transparency (T%), and therefore are promising candidate electrodes materials for a wide range of applications ranging from energy storage to catalysis and electromagnetic interference shielding.[1–9] Moreover, the hydrophilic surface of MXenes allows them to be uniformly dispersed in polar solvents without surfactants or binders that could degrade the σ or T% unlike other 2D materials.[10–12] This trait also facilitates cost-effective large-scale production and aqueous solution processing of MXenes, in contrast to the costly production of conventional transparent conductive electrodes (TCEs) such as indium tin oxides (ITO) and graphene.[13]

However, MXenes have not been evaluated as much as graphene for use as the TCE for optoelectronic applications, mainly because MXenes have poor environmental stability (Figure S1, Supporting Information).[14–17] The insufficient stability results from the hydrophilic surface, which attracts oxygen and water and may lead to oxidation and hydrolysis of the surface.[18–21] The interconnected interlayer spaces between MXene layers form numerous channels for intercalation. MXenes are produced using an exfoliation process, which leaves residual hydrated Li^+ that enlarges the interlayer spacing C that facilitates inward diffusion of water, and this process further increases the C and degrades the electrical properties.[20] Moreover, an electrode requires a high work function (*WF*) to facilitate charge injection in solution-processed optoelectronic devices. Single-component $Ti_3C_2T_x$ MXene TCEs that meet all these requirements (stability, σ, and *WF*) for solution-processed optoelectronics have not been developed yet.

Methods have been evaluated to compensate for the degradation caused by moisture intercalation, but have their own drawbacks. Conductive fillers such as silver nanowires (AgNWs) and conductive polymers can be introduced into $Ti_3C_2T_x$ to form a composite TCE for solution-processed optoelectronics.[22–25] However, this strategy does not address the interactions between MXene and moisture. Reinforcing polymers can be

H. Zhou, S. J. Han, H.-D. Lee, S. H. Jo, T.-W. Lee
Department of Materials Science and Engineering
Seoul National University
Seoul 08826, Republic of Korea
E-mail: twlees@snu.ac.kr

D. Zhang, M. Anayee, Y. Gogotsi
A.J. Drexel Nanomaterials Institute and Department of Materials Science and Engineering
Drexel University
3141 Chestnut Street, Philadelphia, PA 19104, USA
E-mail: gogotsi@drexel.edu

T.-W. Lee
School of Chemical and Biological Engineering
Institute of Engineering Research
Research Institute of Advanced Materials
Soft Foundry
Seoul National University
Seoul 08826, Republic of Korea

The ORCID identification number(s) for the author(s) of this article can be found under https://doi.org/10.1002/adma.202206377.

DOI: 10.1002/adma.202206377

used to increase the hydration resistance of micrometer-thick $Ti_3C_2T_x$ films,[26–28] but this method can significantly degrade σ.

Herein, we present a $Ti_3C_2T_x$ MXene thin film that has a compact structure, combined with a perfluorosulfonic acid (PFSA) barrier layer, as a promising TCE material that has excellent environmental stability, high *WF* of 5.84 eV, and low R_S of 97.4 Ω sq^{-1}. Thermal annealing of pristine $Ti_3C_2T_x$ removes intercalated water, and thereby reduces the interlayer spacing and further impedes the lateral inward diffusion of moisture intercalants. Subsequent surface treatment using PFSA as the barrier layer simultaneously blocks the perpendicular (vertical) diffusion of moisture intercalants between flakes and increases the *WF* from 4.89 to 5.84 eV. This is the highest *WF* ever reported among MXene electrodes and is close to the theoretical upper limit for oxygen-terminated MXene, $Ti_3C_2O_2$.[29] Because of the blockage of paths for rapid moisture diffusion in both lateral and vertical directions, the surface-modified $Ti_3C_2T_x$ exhibits excellent environmental stability with negligible changes in the R_S, and the *WF* maintained at >5.60 eV even after 22 days of exposure to ambient air. MXene electrodes were successfully used as TCEs for both large-area and 10 × 10 passive matrix flexible organic light-emitting diodes (OLEDs) on substrates that measured 6 cm × 6 cm.

2. Results and Discussion

Four types of $Ti_3C_2T_x$ MXene-based TCEs were prepared by spin-coating MXene aqueous dispersions on glass substrates. "Pristine" TCEs were prepared immediately after spin-coating without a rest period. "Closely packed" (*c*-MXene) TCEs were prepared after spin-coating with an initial rest period to allow for self-assembly of $Ti_3C_2T_x$ flakes at the solution-substrate interface; this process increased the uniformity of the thin film without forming any voids and slightly reduced the interlayer spacing. "Highly compact" (*h*-MXene) TCEs were obtained by thermal annealing the *c*-MXene films. "Surface modified" (*m*-MXene) TCEs were prepared by surface-modification of *h*-MXene using PFSA. To test the environmental stability, two electrical contact pads were prepared on each TCE using copper tape to avoid additional contact resistance induced by subsequent layer deposition (**Figure 1**A). The MXene electrodes were then coated by solution processing using water-dispersible poly(3,4-ethylenedioxythiophene):poly(styrenesulfonate) (PEDOT:PSS).

The effects of PEDOT:PSS processing on the electrical properties of the *c*-MXene and *h*-MXene TCEs were evaluated first. Currents *I* through *c*-MXene and *h*-MXene were measured while sweeping voltage *V* from –1 to 1 V before and after PEDOT:PSS coating. For *c*-MXene, the slope of the *I*–*V* curve decreased significantly after PEDOT:PSS coating; this response indicates a severe decrease in the electrical conductivity of $Ti_3C_2T_x$ because of rapid moisture diffusion into the interlayer space (Figure 1B). Direct coating of deionized H_2O on *c*-MXene TCE caused additional degradation in the conductivity (Figure S2A, Supporting Information). However, for *h*-MXene, the *I*–*V* curves changed negligibly after coating with PEDOT:PSS and water; this stability indicates that the resistance to hydration in $Ti_3C_2T_x$ TCEs can be increased by decreasing the interlayer spacing in the MXene (Figure 1C and Figure S2B, Supporting Information).

We propose a mechanism by which these treatments control the resistance of $Ti_3C_2T_x$ to hydration (Figure 1D). Interlayer spacing *C* is equivalent to the *d*-spacing of the stacked layers, minus the thickness of a $Ti_3C_2T_x$ layer (≈1 nm). Pristine MXene has a *C* ≈0.33 nm (detailed results later), which is comparable to the diameter of the hydrated Li^+ ions (≈0.38 nm[30]) that remain

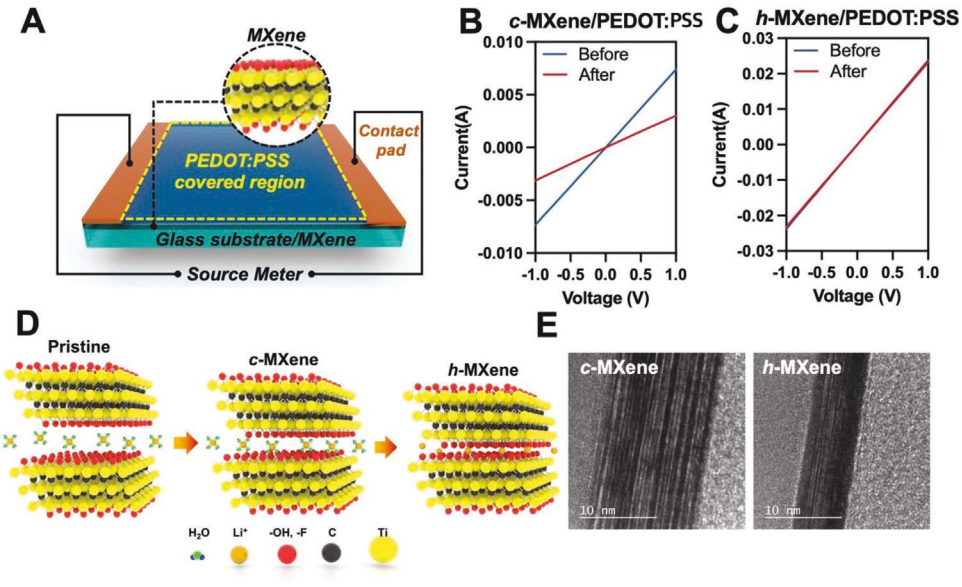

Figure 1. A) Schematic of the $Ti_3C_2T_x$ MXene electrode hydration-stability test. The contact pads were attached to the $Ti_3C_2T_x$ before coating with PEDOT:PSS. B,C) Current versus voltage curves before and after coating with PEDOT:PSS, respectively. D) "Pristine" TCEs were prepared immediately after spin-coating without a rest period. "Closely packed" (*c*-MXene) TCEs were prepared after spin-coating with an initial rest period to allow for self-assembly of $Ti_3C_2T_x$ flakes at the solution–substrate interface. "Highly compact" (*h*-MXene) TCEs were obtained by thermal annealing of *c*-MXene films. E) Transmission electron microscopy (TEM) cross-sectional images of *c*-MXene and *h*-MXene after cutting using a focused ion beam.

as residual species after exfoliation of the multilayer MXene particles to form single-layer MXene sheets. However, to prevent intercalation of water, *C* should be smaller than the size of a water molecule (≈0.275 nm).[20] To preclude lateral diffusion of water between the MXene layers, additional treatments may be necessary.[20] Diffusion of water perpendicularly (with respect to the substrate) between $Ti_3C_2T_x$ flakes also contributes to hydration and should be minimized. A barrier layer on top of the $Ti_3C_2T_x$ layer can block this diffusion path, but doing so without sacrificing the electrical property is challenging and requires an appropriate selection of layer chemistry and processing steps.

High-temperature annealing reduced the *d*-spacing of the $Ti_3C_2T_x$; this result was confirmed using cross-sectional high-resolution transmission electron microscopy (HR-TEM) of *h*-MXene (Figure 1E). This decrease might be a result of the expulsion of intercalated H_2O, surface –—OH groups, or both. The *h*-MXene in several tens of nanomer-scale showed no pores, because the intercalants escaped from the TCE.[2,3] However, *h*-MXene was vulnerable to moisture in the air due to the presence of diffusion paths between $Ti_3C_2T_x$ flakes. Hence, we introduced PFSA as a moisture-diffusion barrier on the surface of *h*-MXene (i.e., *m*-MXene), to improve both charge injection and environmental stability as a TCE.

The thickness-dependent intrinsic electrical and optical properties of *c*-MXenes and corresponding *m*-MXenes after thermal annealing were evaluated to optimize the TCE fabrication (**Figure 2**A,B). Before thermal treatment, the transmittance of $Ti_3C_2T_x$ at 550 nm could be controlled between 38.4% (104.9 nm) and 96.1% (11.3 nm) by adjusting the film thickness. Similarly, R_S could be controlled in the range between 294.0 Ω sq^{-1} (thickness = 11.3 nm) and 18.0 Ω sq^{-1} (104.9 nm), which corresponds to an average conductivity of 5990 S cm^{-1}. After annealing at 350 °C for 6 h, R_S changed from 14.2 (56.4-nm film) to 227.2 Ω sq^{-1} (4.0-nm film), which corresponds to a substantial increase in conductivity from 5990 to 12 252 S cm^{-1} due to removal of water and other intercalants, and due to improved interflake contact.[3]

X-ray diffraction (XRD) was used to quantitatively analyze the structural transformations in $Ti_3C_2T_x$ TCEs after annealing (Figure 2C). The out-of-plane (002) reflection indicative of the MXene flake stacking and interlayer space gradually shifted from a 2θ-angle of 6.64° and 1.33 nm for pristine MXene, to 7.12° and 1.24 nm for *c*-MXene, to 8.26° and 1.07 nm for *h*-MXene, and to 8.32° and 1.06 nm for *m*-MXene (Figure 2D). The substantial reduction in interlayer spacing from ≈0.33 for pristine MXene to ≈0.06 nm for *h*-MXene is due to the removal of water and surface terminations. Moreover, overcoating the TCE with a PFSA barrier layer did not increase the interlayer spacing of $Ti_3C_2T_x$ because the solvent used for the PFSA solution was isopropyl alcohol, which has molecules that are too large to intercalate into the MXene film. This result further supports the stability measurements before and after deposition of PFSA (Figure 1A and Figure S2C,D, Supporting Information). Hence, the resultant *m*-MXene showed excellent stability against subsequent PEDOT:PSS processing (Figure S2E, Supporting Information).

Characterization of the surface morphology of $Ti_3C_2T_x$ TCEs after annealing using atomic force microscopy (AFM) indicated that micron-sized $Ti_3C_2T_x$ flakes are closely packed without islanding or void formation on the substrates (Figure 2E). The line profile across an *h*-MXene sample revealed that each $Ti_3C_2T_x$ layer is ≈1 nm thick. After coating with the PFSA barrier layer, the $Ti_3C_2T_x$ flakes were not visible from the topographic image; this result indicates that PFSA had been deposited uniformly on the surface of the TCEs (Figure 2F). The surface treatment also led to an increase in the WF from 4.89 eV for *h*-MXene to 5.84 eV for *m*-MXene (Figure 2G). Compared with the *WF* of other common TCEs such as ITO (4.70 eV) and AgNW (4.31 eV), the *WF* achieved in this work is most favorable for efficient hole injection, and represents the highest experimentally attained value for $Ti_3C_2T_x$ MXene (Table S1, Supporting Information). Although the thick PFSA (27 nm) could block diffusion of moisture more effectively than the thin layer, the R_S increased from 67.4 (10.7 nm-thick MXene) to 136.8 Ω sq^{-1}, which is fairly high for a TCE (Figure S3, Supporting Information). A thin PFSA layer (6.3 nm) had a relatively low WF of 5.62 eV. Due to the trade-off between *WF* and R_S, MXene with a 10.5 nm-thick PFSA coating (R_S = 97.4 Ω sq^{-1}, *WF* = 5.84 eV) was chosen. Kelvin probe mapping of surface potential in a large area demonstrated the uniformity of the high *WF* after PFSA surface modification (Figure 2H).

The substantial increase in surface potential is mainly induced by the high ionization potential of the perfluoro backbone in the PFSA.[31–33] The *WF* of MXene is strongly dependent on the composition of its surface terminations. For example, the highest theoretically predicted *WF* is ≈6 eV for $Ti_3C_2O_2$ MXene with uniform —O surface terminations.[29] In contrast, the *WF* decreases if the terminations are —OH or —F.[29] Although the surface termination composition can be influenced during MXene synthesis by adjusting the etching method, precise control of the composition is challenging. Thus, achieving a high *WF* for MXenes is a challenging task. Vacuum annealing at elevated temperatures (200 °C) can eliminate the –—OH surface terminations and produce a high *WF* of 5.1 eV.[34] However, surface modification using PFSA provides a simpler and more practical approach than annealing to increase the *WF* of MXene TCE to close to the theoretically predicted maximum.

The stabilities of *c*-MXene, *h*-MXene, and *m*-MXene were evaluated by monitoring the relative changes in resistance *R* with respect to the initial resistance R_0, and the *WF,* after 22 days of exposure to air at room temperature and relative humidity of ≈40% (Figure 2I,J). For *c*-MXene, R/R_0 increased by 37.5% while the *WF* slightly decreased from 4.92 to 4.88 eV. For *h*-MXene, R/R_0 increased by 16.9% while the *WF* remained at ≈4.80 eV; although lateral diffusion of water along the interlayer space was precluded after high-temperature annealing, diffusion of water between $Ti_3C_2T_x$ flakes in the perpendicular direction still affected the hydration stability. For *m*-MXene, R/R_0 increased by only 4.8%, and *WF* maintained at >5.60 eV. Hence, *m*-MXene meets the requirements for stable *R* and high *WF*, and the processing standards of TCEs for OLEDs.

High-resolution X-ray photoelectron spectroscopy was then conducted to analyze the surface oxidation and chemical state of *c*-MXene, *h*-MXene, and *m*-MXene TCEs. For *c*-MXene, the O1s spectrum for the $Ti_3C_2T_x$ was deconvoluted into four components: TiO_2 at 529.4 eV,[3] C–Ti–O at 530.3 eV,[3] Ti–O–Ti at 532.1 eV,[35] and Ti–OH at 532.7 eV[3] (**Figure 3**A). For *h*-MXene, the Ti–OH component contribution to the overall spectra

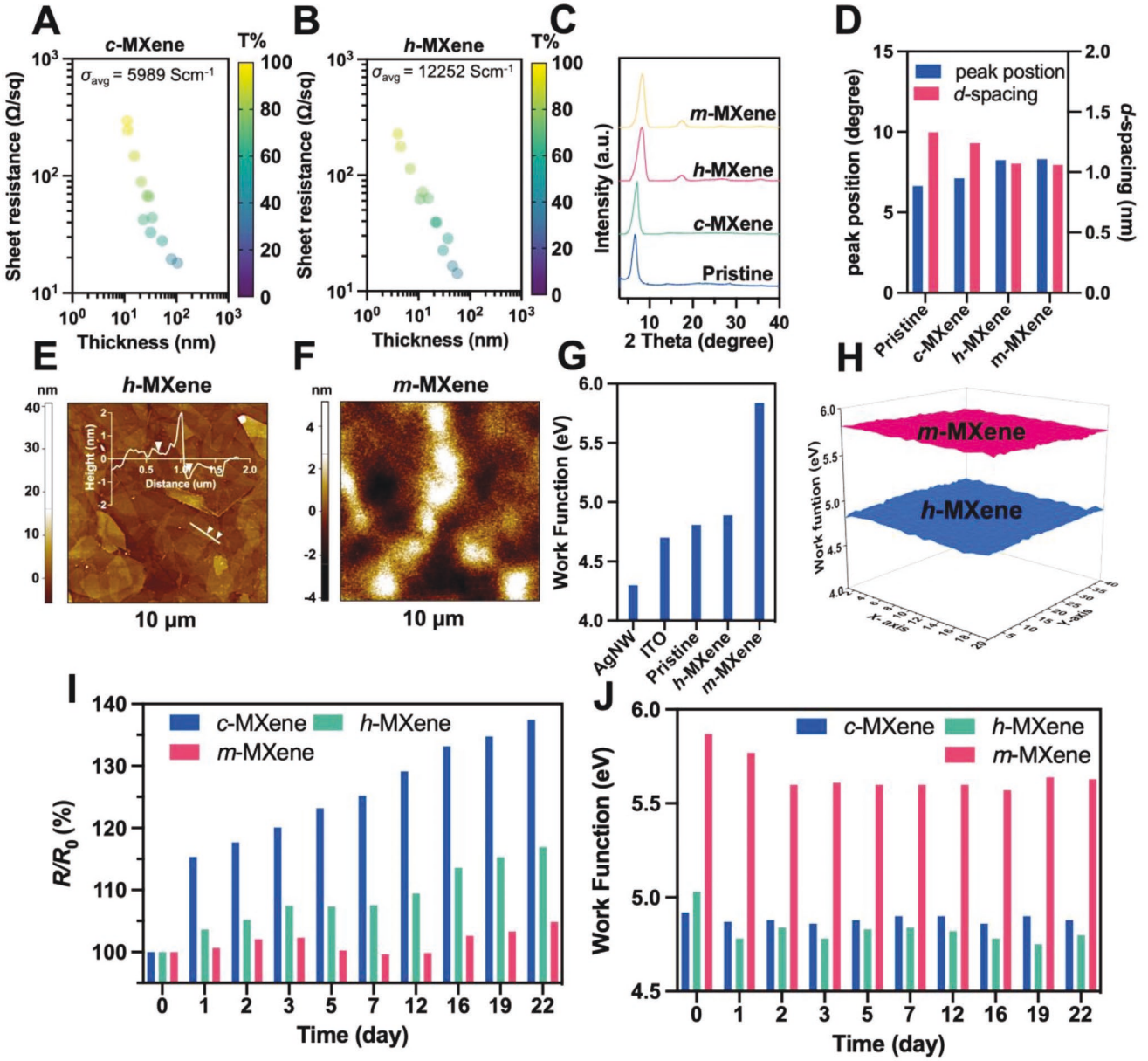

Figure 2. A,B) Thickness-dependent sheet resistance R_S (points) and optical transmittance T% (color scale) of *c*-MXenes (A) and corresponding *m*-MXenes after thermal annealing (B). C) X-ray diffraction pattern (XRD) of pristine, *c*-MXene, *h*-MXene, and surface-modified *h*-MXene (i.e., *m*-MXene) electrodes showing the dominant (002) out-of-plane reflection. D) XRD peak positions extracted from (C) and *d*-spacing calculated based on Bragg's law. E,F) Atomic force microscopy topology images of *h*-MXene (E) and *m*-MXene (F) on a 10 μm scale. G) Work function of electrodes measured using Kelvin probe including silver nanowires (AgNWs), indium tin oxide (ITO), and abovementioned $Ti_3C_2T_x$ electrodes. H) Kelvin probe mapping of *h*-MXene and *m*-MXene electrodes. Each step in the *x*- and the *y*-axis represents 635 nm. I,J) Environmental stability of *c*-MXene, *h*-MXene, and *m*-MXene: changes in sheet resistance (I) and work function (J) at room temperature and relative humidity of ≈40%.

substantially decreased, compared to *c*-MXene; this difference indicates a decrease in the concentration of –OH surface terminations (Figure 3B). Thus, the change in surface chemistry also contributed to the decrease in interlayer spacing as confirmed by HR-TEM and XRD analyses (Figures 1E and 2C,D). However, for *m*-MXene, the Ti–OH component contribution increased slightly (Figure 3C) because the interlayer spacing did not increase after PFSA surface modification, the slight increase in Ti–OH component is likely due to the interaction between PFSA and $Ti_3C_2T_x$ at the interface between them.

Raman spectroscopy was used to analyze the chemical bonding in $Ti_3C_2T_x$ (Figure 3D). Since the vibrational frequency is proportional to the square root of bond strength divided by the effective mass of the atoms connected to the bond, the lattice vibrations are readily affected by the surface groups of MXene layers.[36] The flake region in the Raman spectrum represents the group vibration of carbon along with titanium layers.[6] The shift of the peak in the flake region from 200.1 cm^{-1} for *c*-MXene to 207.3 cm^{-1} for *h*-MXene represents a reduction in the effective mass of the atoms, and further

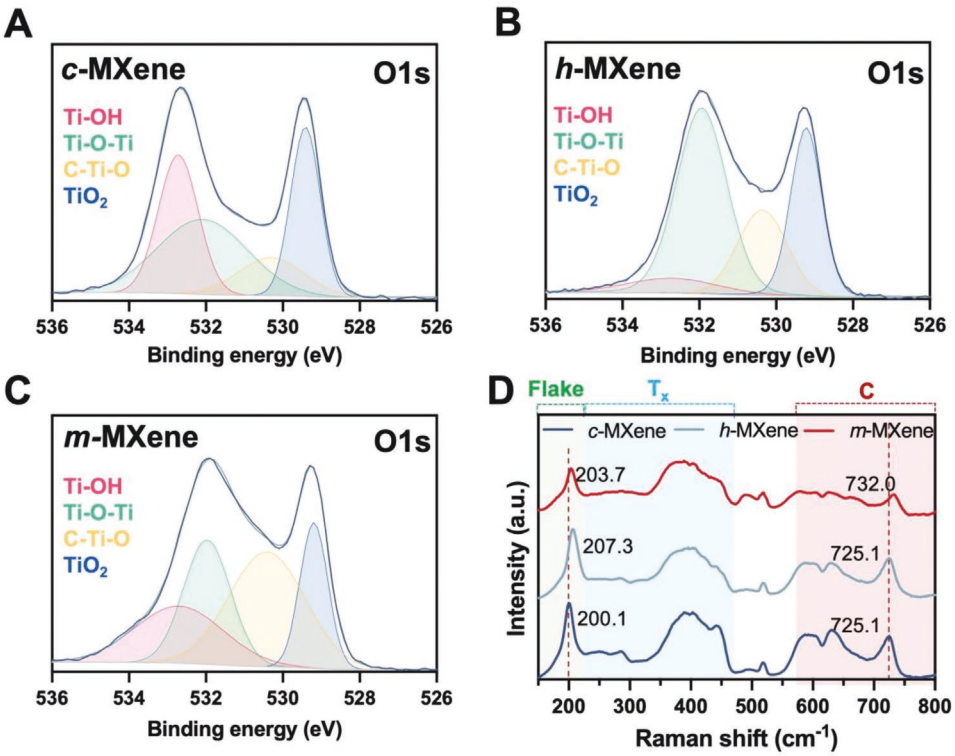

Figure 3. A–C) X-ray photoelectron spectroscopy (XPS) of the O1s core-level for *c*-MXene (A), *h*-MXene (B), and *m*-MXene (C) electrodes. D) Raman spectroscopy of *c*-MXene, *h*-MXene, and *m*-MXene electrodes. Deconvoluted spectra: yellow = flake; blue = surface termination; red = carbon regions.

confirms the removal of -OH surface terminations after high-temperature annealing. After PFSA surface modification, the peak shifted to 203.7 cm^{-1} because of the increase in the effective mass of the atoms because the PFSA film on the $Ti_3C_2T_x$ surface hinders the lattice vibration. These results indicate that the surface groups are effectively removed after high-temperature annealing. The peak position and intensity of *c*-MXene at 725 cm^{-1} in the carbon region remain the same after high-temperature annealing, indicating that the structure of MXenes is well preserved. The peak at 732.0 cm^{-1} in *m*-MXene might be caused by the overcoated PFSA.

To evaluate the electrical characteristics of $Ti_3C_2T_x$ MXene for TCEs, *m*-MXene was used as the anode in a conventional solution-processed OLED in which commercial Super Yellow (PDY-132, Merck) was used as the light-emitting polymer and the final device structure was anode/PEDOT:PSS/Super Yellow/LiF/Al (**Figure 4**A). The OLED fabricated using *m*-MXene as the anode had the highest current densities *J* in the *J*–*V* plots, compared to a reference OLED that used ITO as the anode. Despite the higher σ of ITO ($R_S \approx 10\ \Omega\ sq^{-1}$) compared to *m*-MXene ($R_S = 97.4\ \Omega\ sq^{-1}$), the high *WF* of *m*-MXene substantially facilitates the hole injection, and thereby increases the overall *J*.

The OLEDs showed different luminance versus voltage (*L*–*V*) plots (Figure 4B). All OLEDs had the same device architecture except for the anode material, so the variations result from differences in the hole-injection ability. The maximum luminance L_{max} obtained using *h*-MXene, and *m*-MXene anodes were 34 844 cd m^{-2} at 11.4 V, and 44 243 cd m^{-2} at 10.2 V, respectively, which greatly exceeded the L_{max} obtained using the ITO anode, 6 527 cd m^{-2} at 12.3 V. High L_{max} obtained using *h*-MXene and *m*-MXene implies a highly stable MXene electrode without water-induced degradation caused by solution coating of water-dispersed PEDOT:PSS.

Radiative recombination was also substantially increased due to the increase in hole injection in the *m*-MXene TCE; this increase led to a distinct decrease in efficiency roll-off, and represents a major advantage of *m*-MXene compared with other electrode materials (Figure 4C). Furthermore, the LT_{70} for the initial luminance to decrease to 70% under continuous operation was 25.2 h for the *m*-MXene anode, but 15.1 h for the *h*-MXene anode, and 0.41 h for the ITO anode (Figure 4D).

To demonstrate the scalability of MXenes for optoelectronic devices, *m*-MXene was used as the anode in flexible large-area OLEDs on substrates that measured 6 cm × 6 cm. Instead of the glass substrate used above, the $Ti_3C_2T_x$ MXene was coated on flexible poly(ethylene terephthalate) (PET) substrates and annealed at a lower temperature of 150 °C for 12 h to avoid damage to the PET and to increase the stability of MXene. The XRD diffraction pattern (Figure S4A, Supporting Information) indicates that MXene on PET had a *d*-spacing of 1.1 nm, which corresponds to $C \approx 0.1$ nm, which is small enough to block intercalation of water. The MXene on the PET substrate did not show a decrease in σ induced by water molecules in the PEDOT:PSS aqueous solution (Figure S4B, Supporting Information). Without patterning the anode, the OLED for large-area solid-state lighting was successfully achieved in both inner-bending and outer-bending modes (Figure 4E). This result demonstrates the feasibility of highly uniform *m*-MXenes for large-area applications without water-induced degradation.

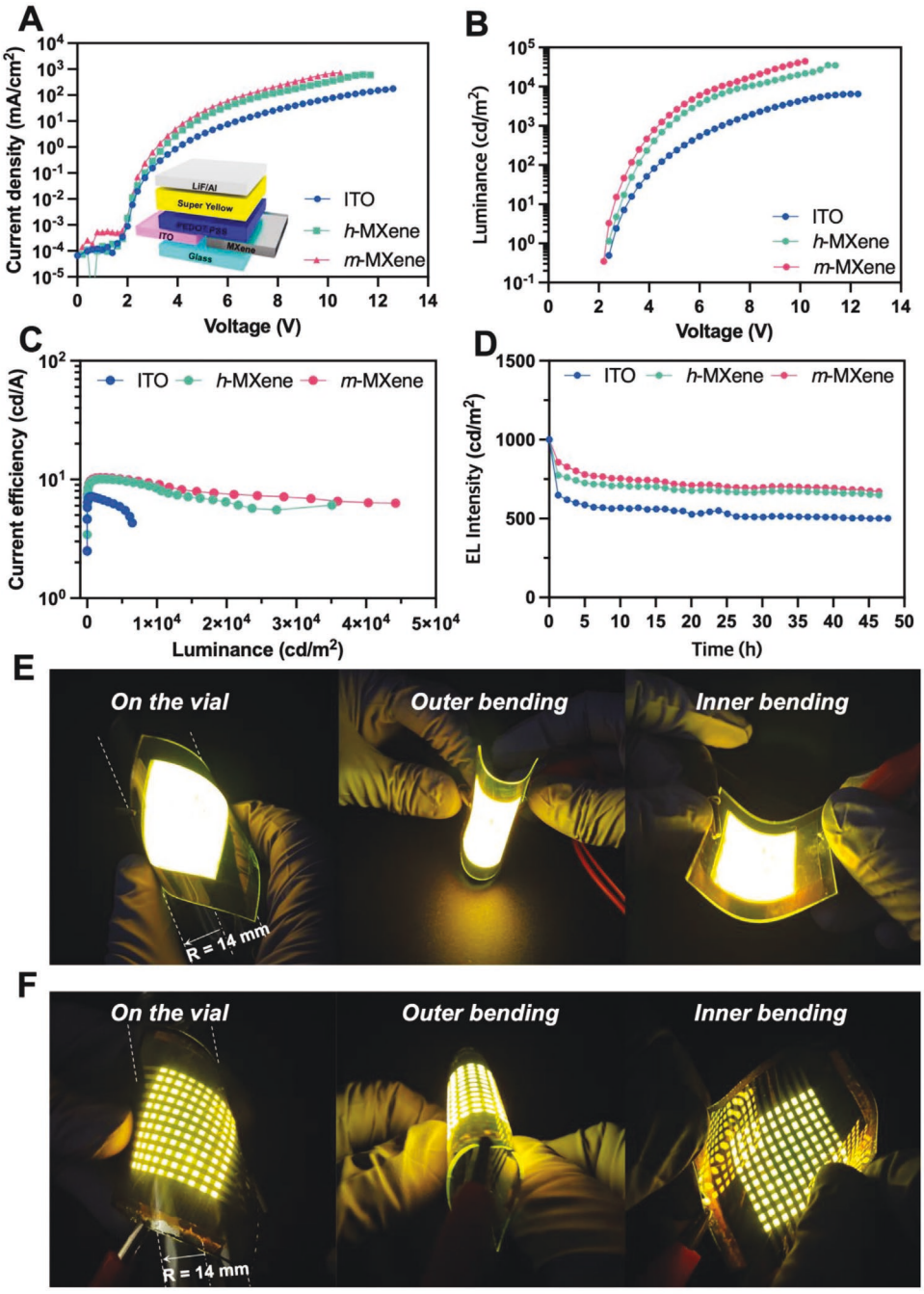

Figure 4. A) Current density vs voltage (*J*–*V*), B) luminance vs voltage (*L*–*V*), C) current efficiency, and D) lifetime (operated at 1000 cd m^{-2} initial luminance) curves for ITO, *h*-MXene, and *m*-MXene-based OLEDs. E,F) Digital photos of *h*-MXene-based large-area solid-state lighting (E) and 10 × 10 passive matrix (F) on PET flexible substrates (6 cm × 6 cm) operated under different mechanical deformations.

Furthermore, a 10 × 10 passive-matrix OLED using *m*-MXene was demonstrated by patterning using a photoresist to make a stripe-type electrode (Figure S5, Supporting Information). The operation of the 10 × 10 passive matrix OLED on 6 cm × 6 cm substrates also proves the high σ of the *m*-MXene and the feasibility of using *m*-MXenes in large area photolithography patterning (Figure 4F). To the best of our knowledge, this is the first use of MXenes for large-area optoelectronics.

3. Conclusion

We have developed a new approach to improve the environmental stability and electrical characteristics of $Ti_3C_2T_x$ MXene TCEs, and then demonstrated their application in large-area optoelectronic devices. The developed $Ti_3C_2T_x$ electrodes simultaneously exhibited excellent environmental stability, high *WF* of 5.84 eV, and low sheet resistance of 97.4 Ω sq^{-1}. High-temperature annealing removed intercalated

water, residual contaminants, and –OH surface terminations to improve the electrical conductivity and increase the *WF*. Moreover, surface treatment with a PFSA layer increased the charge injection, and further increased the *WF*. Combining these approaches can significantly improve the environmental stability by impeding the inward diffusion of moisture in both lateral and perpendicular directions. The *WF* attained herein is the highest ever reported among MXenes and is close to the theoretical upper limit. The developed MXene electrode showed negligible changes in the R_S, and the *WF* remained at >5.60 eV even after 22 days of exposure to air. Finally, solution processing was used to demonstrate flexible large-area and passive-matrix OLEDs on substrates (6 cm × 6 cm). This work provides a simple but effective approach to overcoming the stability limitations of MXenes and is expected to extend their practical applications in large-area optoelectronics.

Supporting Information

Supporting Information is available from the Wiley Online Library or from the author.

Acknowledgements

H.Z., S.J.H., and H.-D.L. contributed equally to this work. This work was supported by National Research Foundation of Korea (NRF) grant funded by the Korea government (Ministry of Science, ICT & Future Planning) (NRF-2016R1A3B1908431), the Pioneer Research Center Program through the National Research Foundation of Korea funded by the Ministry of Science, ICT & Future Planning (NRF-2022M3C1A3081211), and LG Display under LGD-SNU Incubation Program (2021005682). D.Z. and Y.G. were supported by a grant from US National Science Foundation DMR-2041050. M.A. was supported by the US National Science Foundation Graduate Research Fellowship under Grant No. DGE-1646737 and the U.S. Department of Education Graduate Assistance in Areas of National Need (GAANN) fellowship. Any opinions, findings, conclusions or recommendations expressed in this material are those of the author(s) and do not necessarily reflect the views of the National Science Foundation.

Conflict of Interest

The authors declare no conflict of interest.

Data Availability Statement

The data that support the findings of this study are available from the corresponding author upon reasonable request.

Keywords

environmental stability, MXenes, organic light-emitting diodes, perfluorosulfonic acid barrier layers, work function

Received: July 13, 2022
Revised: August 14, 2022
Published online: September 14, 2022

[1] A. V. Mohammadi, J. Rosen, Y. Gogotsi, *Science* **2021**, *372*, eabf1581.
[2] F. Shahzad, M. Alhabeb, C. B. Hatter, B. Anasori, S. M. Hong, C. M. Koo, Y. Gogotsi, *Science* **2016**, *353*, 1137.
[3] A. Iqbal, F. Shahzad, K. Hantanasirisakul, M.-K. Kim, J. Kwon, J. Hong, H. Kim, D. Kim, Y. Gogotsi, C. M. Koo, *Science* **2020**, *369*, 446.
[4] X. Li, Z. Huang, C. E. Shuck, G. Liang, Y. Gogotsi, C. Zhi, *Nat. Rev. Chem.* **2022**, *6*, 389.
[5] Y. Li, H. Shao, Z. Lin, J. Lu, L. Liu, B. Duployer, P. O. Å. Persson, P. Eklund, L. Hultman, M. Li, K. Chen, X.-H. Zha, S. Du, P. Rozier, Z. Chai, E. Raymundo-Piñero, P.-L. Taberna, P. Simon, Q. Huang, *Nat. Mater.* **2020**, *19*, 894.
[6] E. Piatti, A. Arbab, F. Galanti, T. Carey, L. Anzi, D. Spurling, A. Roy, A. Zhussupbekova, K. A. Patel, J. M. Kim, D. Daghero, R. Sordan, V. Nicolosi, R. S. Gonnelli, F. Torrisi, *Nat. Electron.* **2021**, *4*, 893.
[7] B. Anasori, M. R. Lukatskaya, Y. Gogotsi, *Nat. Rev. Mater.* **2017**, *2*, 16098.
[8] W.-T. Cao, F.-F. Chen, Y.-J. Zhu, Y.-G. Zhang, Y.-Y. Jiang, M.-G. Ma, F. Chen, *ACS Nano* **2018**, *12*, 4583.
[9] C. Zhang, B. Anasori, A. Seral-Ascaso, S. H. Park, N. McEvoy, A. Shmeliov, G. S. Duesberg, J. N. Coleman, Y. Gogotsi, V. Nicolosi, *Adv. Mater.* **2017**, *29*, 1702678.
[10] B. Lyu, M. Kim, H. Jing, J. Kang, C. Qian, S. Lee, J. H. Cho, *ACS Nano* **2019**, *13*, 11392.
[11] H. A. Becerril, J. Mao, Z. Liu, R. M. Stoltenberg, Z. Bao, Y. Chen, *ACS Nano* **2008**, *2*, 463.
[12] J. Wu, M. Agrawal, H. A. Becerril, Z. Bao, Z. Liu, Y. Chen, P. Peumans, *ACS Nano* **2010**, *4*, 43.
[13] C. E. Shuck, A. Sarycheva, M. Anayee, A. Levitt, Y. Zhu, S. Uzun, V. Balitskiy, V. Zahorodna, O. Gogotsi, Y. Gogotsi, *Adv. Eng. Mater.* **2020**, *22*, 1901241.
[14] G. S. Lee, T. Yun, H. Kim, I. H. Kim, J. Choi, S. H. Lee, H. J. Lee, H. S. Hwang, J. G. Kim, D.-w. Kim, H. M. Lee, C. M. Koo, S. O. Kim, *ACS Nano* **2020**, *14*, 11722.
[15] H. J. Lee, J. C. Yang, J. Choi, J. Kim, G. S. Lee, S. P. Sasikala, G.-H. Lee, S.-H. K. Park, H. M. Lee, J. Y. Sim, S. Park, S. O. Kim, *ACS Nano* **2021**, *15*, 10347.
[16] T. Yun, H. Kim, A. Iqbal, Y. S. Cho, G. S. Lee, M.-K. Kim, S. J. Kim, D. Kim, Y. Gogotsi, S. O. Kim, C. M. Koo, *Adv. Mater.* **2020**, *32*, 1906769.
[17] T.-H. Han, Y. Lee, M.-R. Choi, S.-H. Woo, S.-H. Bae, B. H. Hong, J.-H. Ahn, T.-W. Lee, *Nat. Photonics* **2012**, *6*, 105.
[18] T. Wu, P. R. C. Kent, Y. Gogotsi, D.-E. Jiang, *Chem. Mater.* **2022**, *34*, 4975.
[19] M. Ghidiu, J. Halim, S. Kota, D. Bish, Y. Gogotsi, M. W. Barsoum, *Chem. Mater.* **2016**, *28*, 3507.
[20] J. Lao, R. Lv, J. Gao, A. Wang, J. Wu, J. Luo, *ACS Nano* **2018**, *12*, 12464.
[21] H. Chen, Y. Wen, Y. Qi, Q. Zhao, L. Qu, C. Li, *Adv. Funct. Mater.* **2020**, *30*, 1906996.
[22] W. Jiang, S. Lee, K. Zhao, K. Lee, H. Han, J. Oh, H. Lee, H. Kim, C. M. Koo, C. Park, *ACS Nano* **2022**, *16*, 9203.
[23] F. Cao, M. You, L. Kong, Y. Dou, Q. Wu, L. Wang, B. Wei, X. Zhang, W.-Y. Wong, X. Yang, *Nano Lett.* **2022**, *22*, 4246.
[24] J. Liu, L. Zhang, C. Li, *Ind. Eng. Chem. Res.* **2019**, *58*, 21485.
[25] S. Bai, X. Guo, T. Chen, Y. Zhang, X. Zhang, H. Yang, X. Zhao, *Composites, Part A* **2020**, *139*, 106088.
[26] Z. Ling, C. E. Ren, M.-Q. Zhao, J. Yang, J. M. Giammarco, J. Qiu, M. W. Barsoum, Y. Gogotsi, *Proc. Natl. Acad. Sci. USA* **2014**, *111*, 16676.
[27] K. Hantanasirisakul, Y. Gogotsi, *Adv. Mater.* **2018**, *30*, 1804779.
[28] M. Han, C. E. Shuck, R. Rakhmanov, D. Parchment, B. Anasori, C. M. Koo, G. Friedman, Y. Gogotsi, *ACS Nano* **2020**, *14*, 5008.
[29] T. Schultz, N. C. Frey, K. Hantanasirisakul, S. Park, S. J. May, V. B. Shenoy, Y. Gogotsi, N. Koch, *Chem. Mater.* **2019**, *31*, 6590.

[30] J. N. Israelachvili, in *Intermolecular and Surface Forces*, 3rd Ed. (Ed: J. N. Israelachvili), Academic Press, San Diego, CA, USA **2011**, p. 71.
[31] H. Zhou, S. J. Han, A. K. Harit, D. H. Kim, D. Y. Kim, Y. S. Choi, H. Kwon, K. N. Kim, G. T. Go, H. J. Yun, B. H. Hong, M. C. Suh, S. Y. Ryu, H. Y. Woo, T. -W. Lee, *Adv. Mater.* **2022**, *34*, 2203040.
[32] S.-J. Kwon, T.-H. Han, T. Y. Ko, N. Li, Y. Kim, D. J. Kim, S.-H. Bae, Y. Yang, B. H. Hong, K. S. Kim, S. Ryu, T.-W. Lee, *Nat. Commun.* **2018**, *9*, 2037.
[33] T.-W. Lee, Y. Chung, O. Kwon, J.-J. Park, *Adv. Funct. Mater.* **2007**, *17*, 390.
[34] S. Ahn, T.-H. Han, K. Maleski, J. Song, Y.-H. Kim, M.-H. Park, H. Zhou, S. Yoo, Y. Gogotsi, T.-W. Lee, *Adv. Mater.* **2020**, *32*, 2000919.
[35] V. Natu, M. Benchakar, C. Canaff, A. Habrioux, S. Célérier, M. W. Barsoum, *Matter* **2021**, *4*, 1224.
[36] A. Sarycheva, Y. Gogotsi, *Chem. Mater.* **2020**, *32*, 3480.